THE JOURNAL OF BIOLOGICAL CHEMISTRY VOL. 288, NO. 26, pp. 18863–18871, June 28, 2013
Published in the U.S.A.

Mutations in the Paxillin-binding Site of Integrin-linked Kinase (ILK) Destabilize the Pseudokinase Domain and Cause Embryonic Lethality in Mice*[S]

Received for publication, March 19, 2013, and in revised form, April 26, 2013 Published, JBC Papers in Press, May 8, 2013, DOI 10.1074/jbc.M113.470476

Daniel Moik[‡], Anika Böttcher[‡], Tatiana Makhina[‡], Carsten Grashoff[§], Nada Bulus[¶], Roy Zent[¶‖], and Reinhard Fässler[‡1]

From the [‡]Department of Molecular Medicine, Max Planck Institute of Biochemistry, 82152 Martinsried, Germany, the [§]Molecular Mechanotransduction Research Group, Max Planck Institute of Biochemistry, 82152 Martinsried, Germany, the [¶]Division of Nephrology, Department of Medicine, Vanderbilt University, Nashville, Tennessee 37232, and the [‖]Department of Medicine, Veterans Affairs Medical Center, Nashville, Tennessee 37232

Background: Integrin-linked kinase is believed to be recruited to focal adhesions (FAs) by binding paxillin via a conserved motif in the pseudokinase domain.
Results: The paxillin-binding motif is not required for FA localization but for ILK stability, parvin and paxillin binding, and mouse development.
Conclusion: ILK does not require paxillin for FA localization.
Significance: Reducing ILK stability perturbs cell migration and development.

Integrin-linked kinase (ILK) localizes to focal adhesions (FAs) where it regulates cell spreading, migration, and growth factor receptor signaling. Previous reports showed that overexpressed ILK in which Val[386] and Thr[387] were substituted with glycine residues (ILK-VT/GG) could neither interact with paxillin nor localize to FA in cells expressing endogenous wild-type ILK, implying that paxillin binding to ILK is required for its localization to FAs. Here, we show that introducing this mutation into the germ line of mice (ILK-VT/GG) caused vasculogenesis defects, resulting in a general developmental delay and death at around embryonic day 12.5. Fibroblasts isolated from ILK-VT/GG mice contained mutant ILK in FAs, showed normal adhesion to and spreading on extracellular matrix substrates but displayed impaired migration. Biochemical analysis revealed that VT/GG substitutions decreased ILK protein stability leading to decreased ILK levels and reduced binding to paxillin and α-parvin. Because paxillin depletion did not affect ILK localization to FAs, the embryonic lethality and the *in vitro* migration defects are likely due to the reduced levels of ILK-VT/GG and diminished binding to parvins.

Integrin-mediated adhesion of cells to extracellular matrix proteins triggers signaling events that govern important cellular processes such as polarity, migration, proliferation, and survival of cells. Because integrin cytoplasmic domains are short and lack catalytic activities, their signaling depends on protein assemblies that form at the adhesion site and are called focal adhesions (FAs).[2] The assembly of FAs is triggered by proteins that bind directly to the cytoplasmic domains of integrin subunits, such as talin, kindlin, paxillin, integrin-linked kinase (ILK), and etc. (1).

ILK is a scaffold protein that consists of five N-terminal ankyrin-like repeats and a C-terminal pseudokinase domain (2). It can either be recruited indirectly to integrin tails through binding kindlins or directly by binding the cytoplasmic domains of β1 and β3 integrins (3). Prior to FA recruitment ILK interacts with the LIM proteins PINCH1 or -2 (encoded by *Lims1* and *Lims2*) (4) and the actin-binding α-, β-, or γ-parvin (encoded by *Parva*, *Parvb*, and *Parvc*) (5) to form the ILK/PINCH/Parvin (IPP) complex. IPP complex assembly is required for FA recruitment and the stability of the individual components (6–8). Upon FA recruitment, the IPP complex associates with F-actin and binds regulators of small GTPases. These properties enable the IPP complex to organize the cytoskeleton during cell spreading, polarization, and migration (9, 10). ILK and its interactors are also implicated in the cross-talk between adhesion- and growth factor receptor-dependent signaling (11, 12), which is essential for cell proliferation, survival, and multiple actin-dependent processes. Genetic studies in mice confirmed these functions. Constitutive loss of ILK abrogates polarity and adhesion of the epiblast resulting in lethality at the peri-implantation stage (13). Tissue-specific ablation identified crucial functions of ILK at later stages of development; ILK gene ablation in keratinocytes for example, revealed adhesion and migration defects and in addition, uncovered a role for anchoring microtubules to FAs required for cell polarity (14, 15). Ablation of the ILK gene in cultured endothelial

* This work was supported by the Max Planck Society (to R. F.); Veterans Affairs Merit Review Grants 1I01BX002196-01, DK075594, DK069221, and DK083187; the O'Brien Center DK79341-01; and an American Heart Association established investigator award (to R. Z.).
[S] This article contains supplemental Tables S1 and S2 and Fig. S1.
[1] To whom correspondence should be addressed: Dept. of Molecular Medicine, Max Planck Institute of Biochemistry, Am Klopferspitz 18, 82152 Martinsried, Germany. Tel.: 49-89-85782424; Fax: 49-89-85792422; E-mail: faessler@biochem.mpg.de.

[2] The abbreviations used are: FA, focal adhesion; IPP, ILK/PINCH/Parvin; E8, embryonic day 8; FN, fibronectin; ILK, integrin-linked-kinase; MEF, mouse embryonic fibroblast; PaxBS, paxillin-binding site; TRITC, tetramethylrhodamine isothiocyanate; TS, Theiler stage.

cells resulted in defective cell spreading, whereas ILK loss in endothelial precursor cells leads to defective vasculogenesis and embryonic lethality between E8.5 and E12.5 (16).

The FA protein paxillin binds directly to α4 integrin tails and indirectly to β-tails through other FA proteins and is also capable of recruiting FA proteins to the adhesion site. Paxillin consists of five leucine and aspartate repeat (LD) motifs followed by four LIM domains (17). Paxillin-null mice die shortly after gastrulation due to defective mesoderm development (18), and paxillin-null cells exhibit defective focal adhesion kinase activation, delayed spreading, shape defects, and impaired migration (18, 19). In a search for paxillin binding motifs in FA proteins, a conserved paxillin-binding site (PaxBS) was identified in α-/β-parvin, ILK, and several other proteins. The binding site of ILK and parvin was mapped to the LD motifs of paxillin. Pulldown experiments with recombinant proteins revealed that co-precipitations of both ILK and α-parvin with paxillin were abolished when their respective PaxBS were mutated. Furthermore, overexpressed PaxBS mutant ILK or α-parvin was unable to localize to FA, whereas paxillin localization was unaffected (20, 21). Although these studies were done in cells that still express endogenous ILK and parvin, the results suggested that paxillin binding through the PaxBS in ILK and parvin is necessary for targeting them to FA. However, recent structural analysis confirmed a direct interaction between paxillin LD repeat-containing peptides and α- or β-parvin but disputed that the proposed PaxBS in parvin represents a counter binding site for paxillin (22–25). Based on these studies, it was proposed that a mutant PaxBS in parvins did not impair paxillin binding but rather the protein fold containing the PaxBS in parvin. Although there is no structural information available detailing the interaction between ILK and paxillin, the PaxBS residues of ILK (Val^{386}/Thr^{387}) were resolved in the ILK pseudokinase domain/α-parvin CH2 domain co-crystal structure (Protein Data Bank code 3KMW) (5). According to this structure, Val^{386}/Thr^{387} are part of the αF helix (residues 370–387) in the C-terminal lobe of the ILK pseudokinase domain and located on the protein surface and therefore principally allow a direct interaction with paxillin (Fig. 1). The side chains of Val^{386}/Thr^{387} are in close proximity (3.2–4.0 Å distance) and thus likely interact with Trp^{383} in the αF helix, Glu^{389} in the F/G loop, Pro^{414} and Ile^{417} in the G/H loop, and Val^{421} and Met^{425} in the αH helix. Trp^{383} in turn seems to stabilize the F/G and G/H loops and thus the αG helix via Pro^{391} and Pro^{411}. It is therefore possible that the substitutions of Val^{386}/Thr^{387} with glycines abolish these interactions, leading to increased flexibility of αF to H helices and their connecting loops. Such a destabilization might result in the unfolding and degradation of the mutant ILK, besides perturbing the interactions with parvin or with paxillin.

To better understand the PaxBS mutation in ILK, we generated and analyzed transgenic mice and cells expressing PaxBS mutant ILK (ILK-VT/GG). Mice homozygous for the mutation die between E8.5 and E12.5 and exhibit general growth retardation, likely caused by defective vasculogenesis. *In vitro* analysis with cells derived from the mutant mice revealed diminished directionality of cell migration. Although PaxBS mutant ILK is normally recruited to FAs, its stability and ability to bind

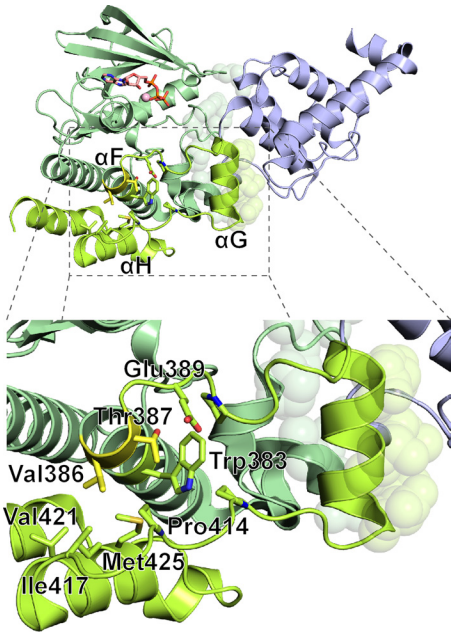

FIGURE 1. **Val^{386}/Thr^{387} in the structure of the ILK pseudokinase/α-parvin CH2 complex.** *A*, schematic representation of Protein Data Bank code 3KMW (5) depicting the pseudokinase domain of ILK (*green*) bound to Mg-ATP (*light red*) and α-parvin CH2 domain (*blue*). C-terminal ILK residues are colored *light green*, and helices αF to αH are labeled. Val^{386}/Thr^{387} side chains are depicted as *yellow sticks*. ILK residues interacting with parvin are depicted as *translucent spheres*. Residues in close proximity of Val^{386}/Thr^{387} are shown in stick representation and labeled in an *inset*, indicated by a *dashed box*.

α-parvin and paxillin were decreased. Depletion or overexpression of paxillin neither altered wild-type or PaxBS mutant ILK protein levels nor their subcellular localization, indicating that the defects caused by the PaxBS mutant ILK occur in a paxillin-independent manner.

EXPERIMENTAL PROCEDURES

Mouse Strains—Mice carrying the ILK-VT/GG substitution were generated as described previously for other ILK mutations (2). In brief, a loxP-flanked neomycin cassette was inserted into exon 13 of the murine ILK gene (13). The GTGACA sequence in exon 12 encoding for valine 386 and threonine 387 was mutated to GGCGGC coding for glycines by site-directed mutagenesis (Stratagene) (supplemental Table S1). The construct was electroporated into R1 ES cells (26). Homologous recombinant clones were identified by Southern blot using genomic DNA with an internal and a 3′ external probe, and by PCR using oligonucleotides PBS-ILK-geno_f and PBS-ILK-geno_r (supplemental Table S1). These oligonucleotides were also used for genotyping using standard methods. Mutant ES cells were injected into C57B6 blastocysts to generate germ line chimaeras. Mutant offspring were intercrossed with deleter-Cre transgenic mice (27) to remove the neomycin cassette. Mice were kept and bred according to Bavarian animal welfare laws in local animal facilities, and they were backcrossed at least seven times to the C57BL/6 genetic background prior to analysis.

Cell Culture—Mouse embryonic fibroblasts (MEFs) were isolated at E9.0 by dissolution of whole embryos with trypsin/EDTA and subsequent plating of cells onto collagen I/fibronec-

tin-coated cell culture dishes. After 16 h of incubation at 37 °C/5% CO_2, cells were infected with SV40-large T transmitting replication incompetent recombinant retrovirus (28). Fibroblasts carrying floxed ILK alleles (ILK-flox) and Adeno-Cre-derived ILK-deficient (ILK-null) cells reconstituted with retroviral wild-type ILK-WT-FLAG constructs were described previously (13). An ILK-VT/GG-FLAG retroviral vector was generated by site-directed mutagenesis and used to transduce low-passage floxed ILK fibroblasts. A cell population without endogenous ILK was obtained by removing the ILK gene using adenoviral Cre recombinase transduction. The loss of endogenous ILK was confirmed by immunoblotting. Cells expressing ILK-WT-Venus and ILK-VT/GG-Venus in the presence or absence of endogenous ILK were created similarly by subcloning ILK-WT or ILK-VT/GG into the retroviral expression vector pLPCXmod-Venus, generating viral supernatants, infecting ILK-flox cells and performing microscopy analysis before and after removing the endogenous ILK gene by adenoviral Cre transduction.

For RNAi-mediated depletion of paxillin, 5′-phosphorylated paxillin-specific (shPxn-sense/-antisense) or scrambled control (shCtrl-sense/-antisense) oligonucleotides (supplemental Table S1) were introduced into the BglII/HindIII-digested pSuper-Retro-puro backbone (Oligoengine). Cells were infected with pSuper-derived virus and selected with puromycin and screened for efficient depletion of paxillin to yield shPxn cells. The human paxillin cDNA was cloned into a retroviral expression vector, and paxillin retrovirus was used to infect shPxn cells to yield shPxn+PXN cells. An mCherry-paxillin cDNA (kindly provided by Lukas Huber, University of Innsbruck) was SLIC-cloned (29) into a vector with ITRs for Sleeping beauty transposase and IRES (internal ribosomal entry site)-hygromycin-resistance (pSB-ITR_CAG-IRES-hygroR, kindly provided by Marc Schmidt-Supprian, Max Planck Institute of Biochemistry). Cells were subsequently co-transfected with Sleeping Beauty 100× expression vector (30), selected with hygromycin for Cherry-paxillin expression, and maintained in minimal medium (DMEM containing 4.5 g/liter D-glucose, 0.8 g/liter L-alanyl-L-glutamine, 100 units/ml penicillin, 100 mg/liter streptomycin) or growth medium (minimal medium plus 10% FCS. Unless otherwise noted, all cell culture reagents were reagent grade from Invitrogen or Sigma.

Adhesion, Spreading, and Migration Assays—Assays were performed as described previously (31). Briefly, cell adhesion was determined with a plate-and-wash assay where cells were allowed to adhere for 30 min at 37 °C on decreasing amounts of fibronectin (FN, Calbiochem), followed by washing and colorimetric detection of adherent cells at 280 nm. Measurements were performed in quadruplets. Spreading assays were performed by adding cells onto FN-coated eight-well chamber slides followed by careful addition of paraformaldehyde/PBS at defined times for fixation. Fixed cells were fluorescently stained with phalloidin-TRITC and DAPI to allow visualization of cellular and nuclear area. 100 random fields of view (10×/0.4 numerical aperture objective) per time point were analyzed using ImageJ software. A random field typically contained 2–10 cells.

Random migration was performed at 37 °C/5% CO_2 using a live cell imaging setup with one picture taken every 5 min. For random migration assays, sparsely seeded non-dividing polarized cells were tracked for 6 h (20×/0.4 numerical aperture objective). Cell tracking was performed with ImageJ software and the cell tracking add-on (32), whereas cell velocity and directionality were computed using the chemotaxis and migration tool (version 2.0, Ibidi). Directionality is the quotient of actual and Euklidian distance of a cell track. Haptotactic cell migration was assayed as described previously (33). Transwells with 8-μm pores were coated with fibronectin (0.5 μg/ml), and 1×10^5 cells were added to the upper well in serum-free medium. Cells that migrated through the filter after 4 h were counted and are expressed as migrated cells per high power field (400×).

Antibodies—Primary antibodies used for immunoblotting, immunofluorescence, or flow cytometry are detailed in supplemental Table S2. Appropriate HRP- or fluorophor-conjugated secondary antibodies were obtained from Bio-Rad or Jackson ImmunoResearch Laboratories.

Flow Cytometry—Flow cytometry measurements were performed as described previously (34). Briefly, cells were trypsinized and stained with primary antibodies for 10–30 min on ice, washed, and stained with secondary antibody for 10–30 min on ice. After washing, cells were resuspended in 0.5% (w/v) BSA/PBS. Flow cytometry was performed in triplicates with a FACSCalibur flow cytometer (Becton & Dickinson).

Immunofluorescence—Cryo-sections of 8-μm thickness from embryonic tissues were prepared and embedded according to standard protocols. Cells were grown on glass-coated with 5 mg/liter FN. Samples were either paraformaldehyde-fixed (10 min in 3.7% paraformaldehyde/PBS, permeabilized 3 min with 0.1% Triton X-100/PBS) or methanol/acetone fixed (twice 5 min with ice-cold methanol/acetone 1:1, air drying). Tissue sections were blocked for 1 h in 5% BSA/PBS and then treated with 0.1% Triton X-100/PBS for 20 min, and cells were blocked for 1 h in 1% BSA/0.1% Triton X-100/PBS. Primary antibodies were diluted in blocking solution and applied overnight at 4 °C. After washing with PBS, appropriate secondary antibodies were diluted in blocking solution and applied for 1 h at room temperature. After washing and DAPI staining (1:10,000 in PBS), slides were mounted in Elvanol. Pictures were taken with a TCS SP5 AOBS confocal laser scanning microscope (Leica). All stainings were repeated at least three times.

Western Blotting and Immunoprecipitations—Cells or embryos were homogenized in 150 mM NaCl, 50 mM Tris-HCl, 5 mM EDTA, 0.1% w/v SDS, 1.0% (w/v) sodium deoxycholate, 1.0% (v/v) Triton X-100, phosphatase inhibitor cocktails P1 and P2, pH 7.6; all by Sigma) supplemented with Complete protease inhibitors (Roche Applied Science), followed by sonication for 30 s at 4 °C. Equal amounts of total protein per lane were separated on a polyacrylamide gel and transferred to PVDF membranes (Millipore). Membrane blocking and antibody dilution was performed with TBS, pH 7.6, supplemented with 0.1% Tween 20 (Serva) and 2% skim milk (Fluka) or 5% BSA (PAA Laboratories). Subsequently, membranes were incubated for 1 h at room temperature or overnight at 4 °C with primary

TABLE 1
Mendelian ratio of offspring derived from $ILK^{+/ki}$ intercrosses at birth

No. of offspring	Genotype	Real (ideal) percentage	$p(Chi^2)$[a]
287	$ILK^{+/+}$	31% (25%)	1×10^{-21}
	$ILK^{+/ki}$	69% 50%)	1×10^{-21}
	$ILK^{ki/ki}$	0% (25%)	1×10^{-21}

[a] The Chi-square test in this column compares the real with ideal Mendelian allele distributions.

antibody. After washing, appropriate HRP-coupled secondary antibodies (Bio-Rad) were applied for 1 h at room temperature. After final washing, ECL detection (Immobilon, Millipore) was performed at a LAS4000 (Fujifilm). Images were analyzed with ImageJ software for quantification. All stainings were repeated at least three times.

For immunoprecipitation of FLAG-tagged ILK, cells were starved overnight and then plated for 4 h on FN-coated dishes. After lysis in 10 mM Tris-HCl, 50 mM NaCl, 10% (v/v) glycerol, 1%(v/v) Igepal C630 and inhibitors as above, pH 7.6, on ice, cells were sonicated, debris was pelleted, and 1.0 mg of total protein was immunoprecipitated using M2-anti-FLAG resin (Sigma). After washing and elution, co-immunoprecipitated protein was visualized by Western blotting.

Statistics—All experiments were repeated at least three times. All numerical data are given as mean value with S.D. or S.E. For S.E., the number of biological replicates used is indicated in the figure legend. Statistical significance was tested by two-tailed Student's *t* or Chi square test.

RESULTS

$ILK^{ki/ki}$ Embryos Display a General Growth Retardation and Die Before E12.5—We generated ILK+/(VT/GG) knock-in mice (abbreviated $ILK^{+/ki}$) by homologous recombination in ES cells as described previously (2) (supplemental Fig. S1, *A–D*). $ILK^{+/ki}$ mice were viable, fertile, and indiscernible from their wild-type littermates. Heterozygous intercrosses failed to produce homozygous $ILK^{ki/ki}$ mice at birth, indicating that the mutation is embryonic lethal (Table 1). To identify the time of lethality, we performed timed matings and staged isolated embryos by developmental hallmarks and somite pair numbers according to Theiler (35). Between embryonic day (E) 8.0 and 12.5 there were only sporadic embryonic resorptions of controls ($ILK^{+/+}$ and $ILK^{+/ki}$) (Table 2). $ILK^{ki/ki}$ embryos developed normally to Theiler stage (TS) 11 corresponding to E8.0. However, after this stage, an increasing percentage was resorbed, and at E12.5, no live $ILK^{ki/ki}$ embryos could be isolated (Table 2).

At E8.0, control and $ILK^{ki/ki}$ embryos were in the late neural plate/early head-fold stage of development (TS 11a-c). The amnion was not fully closed in ~20% of $ILK^{ki/ki}$ embryos, indicating a slight delay in development compared with controls. Although almost all E8.5 control embryos were in the late preturning (TS 12b) or turning stage (TS 13), the majority of E8.5 $ILK^{ki/ki}$ embryos were still in head-fold (TS 11c/d) or early preturning stages (TS 12a) (Table 3). Despite the general retardation, organogenesis, *e.g.* of the heart was normal (Fig. 2*A*). At E9.5, wild-type embryos had completed turning and were forming and closing the anterior neuropore (TS 15), whereas 95% of the E9.5 $ILK^{ki/ki}$ embryos were either in the midst of or just finished turning (TS 13/14) (Fig. 2*A*). After E9.5, most $ILK^{ki/ki}$ embryos were either in the process of being resorbed or showed a pronounced delay compared with control littermates.

Although the general delay in development of $ILK^{ki/ki}$ embryos implies pleiotropic defects, the most striking abnormality was the absence of a vasculature on $ILK^{ki/ki}$ yolk sacs at E9.5 and later (Fig. 2*B*). To define the vascular abnormality in more detail, we investigated yolk sac vasculogenesis at E8.5 and 9.5. In E8.5 controls, precursor cells originating from proximal cavernous blood islands gave rise to a distal primitive vascular plexus close to the embryo proper and demarcated by a continuous FN-containing basement membrane (Fig. 2*C*). Although FN staining revealed that $ILK^{ki/ki}$ yolk sacs also contained proximal blood islands, they lacked discernible distal vascular structures (Fig. 2*C*). At E9.5, the presence of veins, arteries, and capillaries indicated angiogenic remodeling in control yolk sacs. However, $ILK^{ki/ki}$ yolk sacs only displayed a dilated primitive plexus and no discernible arteries, veins, and capillaries (Fig. 2*D*).

To test whether the ILK-VT/GG mutation allowed integrin-mediated assembly of basement membranes, we performed immunofluorescence stainings for FN and laminin in the embryonic neuroectoderm (Fig. 2*E*). Control and $ILK^{ki/ki}$ embryos showed normal basement membrane assembly without blisters or other cell adhesion defects such as basement membrane splitting. Taken together, these data show that $ILK^{ki/ki}$ embryos display a general delay in their development after E8.0 with defective vasculogenesis and death between E8.5 and E12.5. The normal formation of blood islands indicates that early hematopoietic development was normal in $ILK^{ki/ki}$ yolk sacs, whereas the subsequent establishment of the vascular plexus was delayed.

$ILK^{ki/ki}$ Cells Have a Migration Defect—The formation of the primitive vascular plexus crucially depends on the migration of endothelial precursor cells that originate from yolk sac blood islands and migrate to the distal yolk sac regions (36). We therefore decided to test whether the $ILK^{ki/ki}$ mutation affects cell migration. Because we could not obtain enough endothelial cells from yolk sac tissues, we isolated and immortalized embryonic cells (MEFs) from E9.0 control and $ILK^{ki/ki}$ embryos. $ILK^{ki/ki}$ MEFs showed normal surface expression levels for $\beta1$, $\beta3$, αV, and $\alpha5$ integrins as well as normal cell attachment and spreading (Fig. 3, *A–C*). Consistent with these observations, we found that immediate integrin-dependent signaling such as focal adhesion kinase and AKT phosphorylation were similar in control and $ILK^{ki/ki}$ cells following plating on FN (Fig. 3*D*). However, we found that $ILK^{ki/ki}$ MEFs have a significantly reduced capacity to transmigrate through FN-coated porous Transwell membranes ($p < 0.001$) (Fig. 3*E*). To determine whether this defect is due to decreased migration velocity or directionality, we performed random migration assays and found that migration velocities of $ILK^{ki/ki}$ MEFs were increased, whereas the directionality of migration was decreased (Fig. 3*F*). Thus, the developmental vasculogenesis defects likely arise from directional migration defects of endothelial precursor cells.

TABLE 2

Mendelian ratios determined at different stages of embryogenesis

Shown is the number of embryos resulting from timed $ILK^{+/ki}$ intercrosses harvested at indicated days of embryogenesis. Unknown genotype refers to resorbing embryos where genotyping was impossible. Embryo numbers are given by genotype as normal/delayed/resorbing embryos. Normal refers to embryos comparable with the majority of littermates; delayed denotes embryos at least one stage behind the majority of littermates; resorbing refers to genotypeable embryonic resorbates. p(all,Chi^2) gives the result of a Chi square test with ideal Mendelian inheritance of all genotypeable embryos, p(normal, Chi^2) excludes delayed and resorbing embryos.

	Embryos (unknown genotype)	$ILK^{+/+}$	$ILK^{+/ki}$	$ILK^{ki/ki}$	p (all, Chi^2)	p (normal, Chi^2)
E8.0	35 (6)	9/0/0	15/0/0	4/1/0	0.70	0.38
E8.5	215 (17)	41/7/1	100/7/3	9/22/8	0.18	2.6×10^{-7}
E9.5	111 (11)	25/2/2	40/8/1	2/14/6	0.60	1.1×10^{-4}
E10.5	75 (3)	20/0/0	36/0/0	1/12/3	0.80	2.5×10^{-4}
E12.5	70 (17)	15/0/1	27/0/1	0/0/9	0.36	8.5×10^{-4}

TABLE 3

Theiler staging determined from E8.5 litters of $ILK^{+/ki}$ intercrosses

E8.5 embryos from timed $ILK^{+/ki}$ intercrosses were staged according to Theiler and then genotyped.

TS	$ILK^{+/+}$	$ILK^{+/ki}$	$ILK^{ki/ki}$
11b	0	1	1
11c	0	1	4
11d	8	10	4
12a	4	16	8
12b	17	35	6
13	10	11	2

The Stability of ILK-VT/GG Protein Is Reduced—To discern how the ILK-VT/GG mutation caused the cellular migration defect, we performed a biochemical characterization of IPP and paxillin expression levels by immunoblotting. IPP protein levels were severely reduced in both $ILK^{ki/ki}$ embryos and MEFs compared with controls, whereas paxillin levels were unchanged (Fig. 4, *A* and *B*). Because reduced stability of the ILK-VTGG protein could explain the observed reduction in PINCH and α-parvin levels, we treated control and $ILK^{ki/ki}$ MEFs with cycloheximide to inhibit protein synthesis and monitored the decrease of ILK levels over time. Control MEFs displayed a 22 ± 2% reduction of ILK after cycloheximide treatment for 20 h (Fig. 4*C*). In contrast, $ILK^{ki/ki}$ MEFs showed a 58 ± 23% reduction in ILK-VT/GG levels, indicating that the protein turnover of the mutant ILK was 2.6-fold increased in $ILK^{ki/ki}$ cells (p = 0.005) (Fig. 4*C*). By comparison, the reduction of β1 integrin was similar in both cell lines (50 ± 17% *versus* 50 ± 9%, p = 0.97) (Fig. 4*C*), indicating that the increased turnover of ILK-VT/GG was specific.

It has been reported that ILK-VT/GG was unable to localize to FAs when ectopically expressed in various cell lines (20, 21). To confirm this finding in $ILK^{ki/ki}$ MEFs, we plated MEFs on FN and visualized ILK, parvin, and paxillin by immunostaining. Unexpectedly, all three proteins localized normally to FAs in both wild-type and $ILK^{ki/ki}$ MEFs (Fig. 4*D*). To test whether endogenous wild-type ILK interferes with FA localization of ILK-VT/GG, we stably transduced either ILK-WT or ILK-VT/GG fused to the fluorophor Venus into ILK-floxed cells expressing endogenous ILK. An aliquot of these cells was used to transiently express the Cre recombinase, which deleted the endogenous ILK and yielded ILK-null cells overexpressing either of the two constructs. When examining the localization of Venus-tagged ILK proteins, we observed ILK-WT in FAs as shown by Vinculin co-localization both in cells expressing or lacking endogenous ILK (Fig. 4*E*). Remarkably, although ILK-VT/GG localized to FA in the absence of endogenous ILK, it failed to localize to FAs in the presence of endogenous ILK (Fig. 4*E*). This confirms the hypothesis that endogenous ILK interferes with ILK-VT/GG recruitment to FAs. Taken together, these data show that the ILK-VT/GG mutation decreases the stability of the IPP complex without affecting paxillin levels or localization.

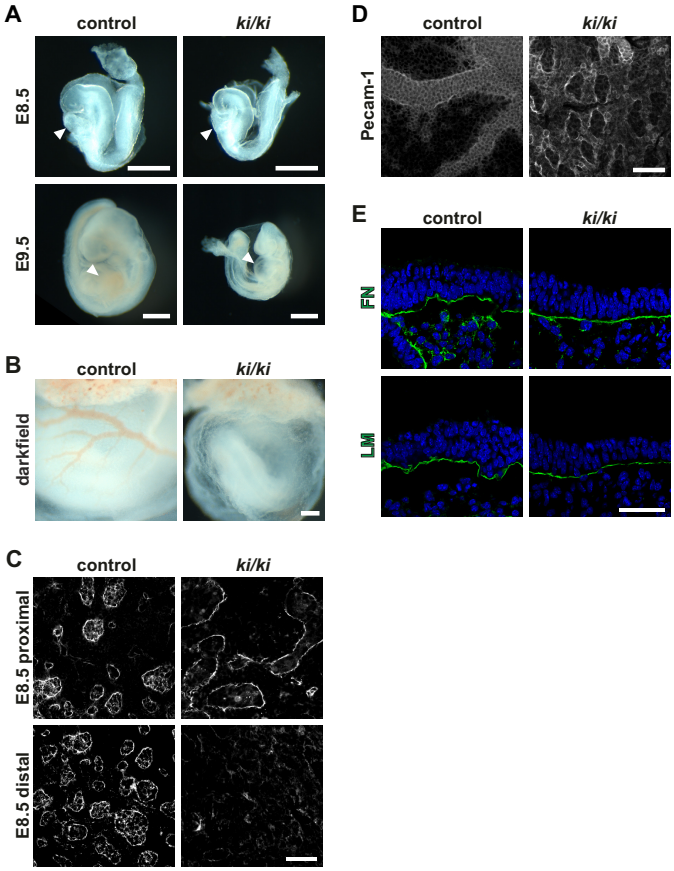

FIGURE 2. **$ILK^{ki/ki}$ embryos display developmental delays and defective yolk sac vasculogenesis.** *A*, representative control or $ILK^{ki/ki}$ (*ki/ki*) E8.5 (TS 12b, 12a) and E9.5 (TS 15, 14) embryos. *Arrowheads* indicate the heart. *B*, dark field picture of representative E9.5 control and $ILK^{ki/ki}$ yolk sacs. *C*, FN immunofluorescence staining of proximal or distal E8.5 control or *ki/ki* yolk sac whole mounts. *D*, PECAM-1 immunofluorescence staining of E9.5 control or *ki/ki* yolk sac whole mounts. *E*, FN or pan-laminin (*LM*; *green*) immunofluorescence staining of E8.5 embryonic neuroectoderm. Nuclei were DAPI-stained (*blue*). *Scale bar*, 200 μm (*A*) and 50 μm (*B–D*).

Overexpression of ILK-VT/GG Fails to Normalize Parvin Levels and Migration—Our data suggest that the mutation of the PaxBS in ILK leads to overall instability of the protein, which in turn decreased levels of PINCH and α-parvin. To test whether elevated ILK-VT/GG levels would normalize IPP and migration, we stably overexpressed FLAG-tagged WT or ILK-

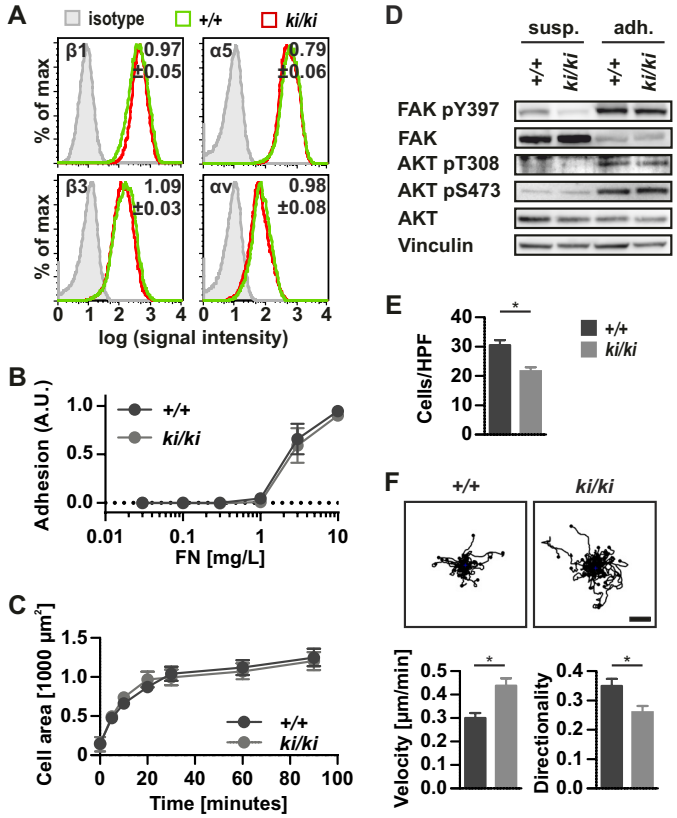

FIGURE 3. **ILK$^{ki/ki}$ cells display impaired transwell migration due to reduced directionality of migration.** *A*, flow cytometry analysis for integrin β1, β3, α5, and αV surface expression of on +/+ (*green*) and *ki/ki* (*red*) MEFs (*solid gray*, isotype control). *Numbers* indicate the ratio of mean fluorescence intensity in *ki/ki* over +/+ MEFs (mean ± S.E., $n = 3$). *B* and *C*, representative cell adhesion assay (*B*) and spreading kinetics (*C*) on FN with +/+ (*dark gray*) and *ki/ki* (*light gray*) MEFs. The *line* indicates mean ± S.D. (*B*) or S.E. ($n = 3$; *C*). *A.U.*, Absorption Units. *D*, immunoblot analysis for the indicated proteins in suspended (*susp.*) or FN-adherent (*adh.*) +/+ or *ki/ki* MEFs. *E*, Transwell migration assays of +/+ and *ki/ki* MEFs through FN-coated membranes with 8-μm pore size. *Bars* indicate mean ± S.E. ($n = 3$) cells per phase contrast high-power-field (*HPF*) that migrated through the membrane in 4 h. *, $p < 0.05$. *F*, random migration assay of +/+ (*dark gray*) and *ki/ki* (*light gray*) MEFs. *Top panel*, cell tracks used for analysis. *Scale bar*, 50 μm. *Bottom panel*, migration velocity (in μm/min) and directionality, color coded as described above. *Columns* indicate mean ± S.E. ($n = 3$); *, $p < 0.03$.

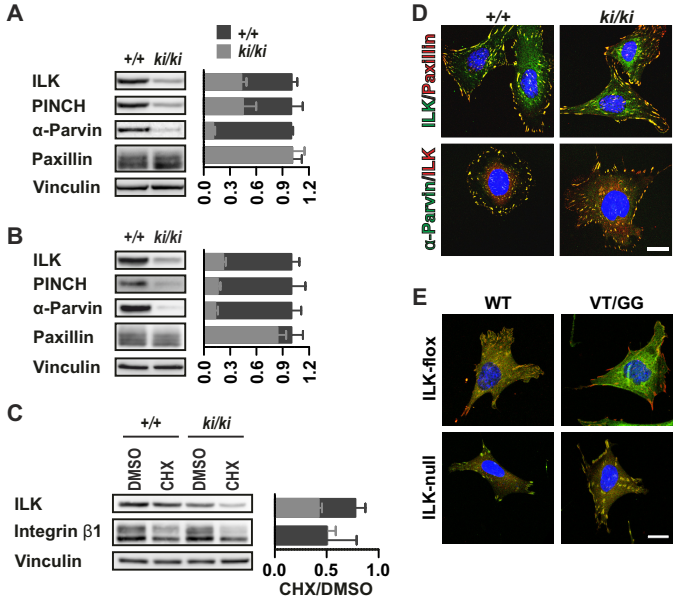

FIGURE 4. **Mutant ILK is turned over faster but localizes to FA and permits normal FA signaling.** *A* and *B*, immunoblot of analysis for the indicated proteins in control or *ki/ki* lysates ($n = 3/3$) of E8.5 embryos (*A*) or mouse embryonic cells (MEFs) (*B*). *Bars* indicate mean ± S.E. ratio of signal in *ki/ki* (*light gray*) over control (*dark gray*) samples, normalized to vinculin. *C*, immunoblot (*IB*) analysis for the indicated proteins in +/+ or *ki/ki* MEFs treated for 20 h with vehicle control (dimethyl sulfoxide (*DMSO*)) or with the ribosomal inhibitor cycloheximide (*CHX*). *Bars* indicate mean ± S.E. ($n = 3$) ratio of signal of cycloheximide- over vehicle-treated +/+ (*dark gray*) or *ki/ki* (*light gray*) MEFs, normalized to vinculin. *D*, immunofluorescence stainings of +/+ and *ki/ki* MEFs for the indicated proteins, colors (*green/red*) indicate false color used in the images. Nuclei were DAPI-stained (*blue*). Picture acquisition was optimized for optimal signal and does not reflect reduced protein levels in *ki/ki* MEFs. *Scale bar*, 20 μm. *E*, immunofluorescence stainings for GFP (*green*) and vinculin (*red*) of ILK-flox or ILK-null fibroblasts stably transduced with ILK-WT or ILK-VT/GG fused to the fluorophor Venus. Nuclei are stained with DAPI (*blue*). *Scale bar*, 20 μm.

VT/GG in ILK-null fibroblasts. This allowed us to increase ILK-WT levels to 4.2 times and ILK-VT/GG to 2.6 times when compared with the amount of endogenous ILK in parental ILK-floxed cells (Fig. 5*A*). Although PINCH levels increased concomitantly with ILK-VT/GG, α-parvin levels remained low. The levels of paxillin and of the HSP90, which was shown to stabilize ILK by binding the pseudokinase domain (37), were similar in all cell lines analyzed. Consistent with the inability to normalize α-parvin levels, ILK-VT/GG overexpressing cells showed the same migration defects as *ILK$^{ki/ki}$* MEFs (Fig. 5*B*), whereas adhesion was normal (Fig. 5*C*). Taken together, these results suggest that elevating ILK-VT/GG levels rescued PINCH, but not parvin levels or the migration defect.

ILK-VT/GG Binds Less α-Parvin and Paxillin—ILK protein is stabilized by binding PINCH, parvin, and HSP90 (6–8, 37). The reduced ILK-VT/GG stability raises the possibility that binding to these interactors is impaired. We tested this hypothesis by determining the amounts of bound interactors using anti-FLAG immunoprecipitation followed by immunoblotting (Fig. 5*D*). PINCH, which binds the ankyrin repeat domains, and HSP90 were co-immunoprecipitated to a similar extent in ILK-WT and ILK-VTGG-expressing cells. In contrast, co-immunoprecipitation of α-Parvin was severely diminished. Because ILK, PINCH, and parvin protein levels depend on each other, decreased parvin binding by ILK-VT/GG could cause the reduction of IPP protein levels in *ILK$^{ki/ki}$* cells. Interestingly, the ILK-VT/GG mutation reduced but did not abolish paxillin binding. The reduced amounts of paxillin in ILK-VT/GG precipitates point to either an impaired direct binding of paxillin to ILK-VT/GG or alternatively reduced indirect binding to ILK-VT/GG due to less co-precipitated parvin.

Depletion or Overexpression of Paxillin Does Not Affect Levels or Localization of ILK—If reduced paxillin binding to ILK-VT/GG was responsible for the instability of the mutant ILK protein, depletion of paxillin levels should destabilize ILK-WT. To test this hypothesis, we depleted paxillin in ILK-floxed cells by RNAi with a paxillin-specific shRNA (shPxn) and also rescued the shPxn cells by re-expressing a shPxn-resistant human *PAXILLIN* cDNA (shPxn+PXN). Control cells expressed scrambled control shRNA (shCtrl). The shPxn depleted endogenous paxillin by 97% and re-expression of human PAXILLIN resulted in a 13-fold increase in protein levels (Fig. 6*A*). Using an anti-paxillin antibody with cross-reactivity against Hic-5, we failed to detect a specific signal in immunostainings of shPxn

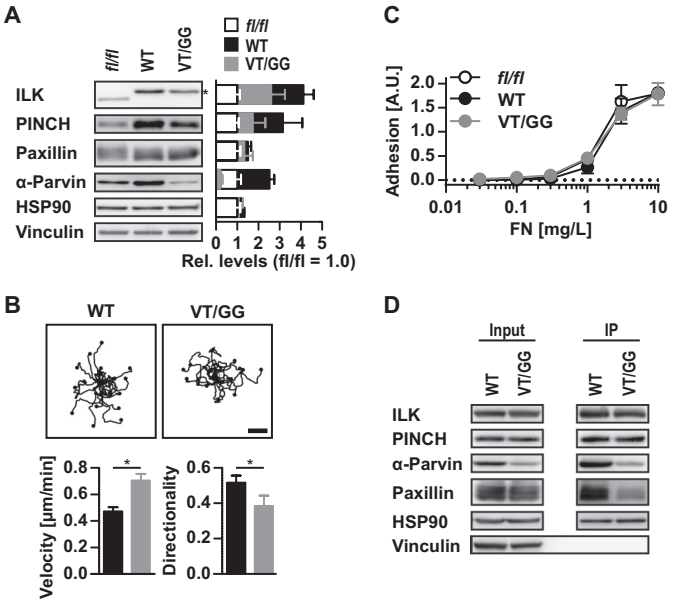

FIGURE 5. **Mutant ILK has reduced parvin and paxillin binding capacity and cannot rescue cell migration defects or reduced parvin protein levels.** *A*, immunoblot analysis for the indicated proteins in ILK-floxed (*fl/fl*, *white*) fibroblasts and in ILK-null fibroblasts stably expressing FLAG-tagged WT ILK (*dark gray*) or mutant ILK (VT/GG, *light gray*). The *asterisk* indicates transgenic ILK-FLAG. *Bars* indicate mean ± S.E. ($n = 3$) ratio of protein in WT (*dark gray*) or VT/GG (*light gray*) fibroblasts, normalized to vinculin and relative to ILK-floxed cells (*white*). *Rel.*, relative. *B*, random migration assay of WT and VT/GG fibroblasts. *Top panel*, cell tracks used for analysis. *Scale bar*, 50 μm. *Bottom panel*, migration velocity (in μm/min) and directionality of WT (*dark gray*) and VT/GG (*light gray*) fibroblasts. *Bars* indicate mean ± S.E. ($n = 3$); *, $p < 0.02$. *C*, representative cell adhesion assay on FN with ILK-floxed (*fl/fl*, *white*), WT (*dark gray*), or VT/GG (*light gray*) cells. The *line* indicates mean ± S.D. *A.U.*, absorption units. *D*, anti-FLAG immunoprecipitation (*IP*) for ILK and immunoblot analysis for the indicated proteins in WT and VT/GG cells. Whole cell lysates (*Input*) and immunoprecipitation lanes are indicated. *L*, liter.

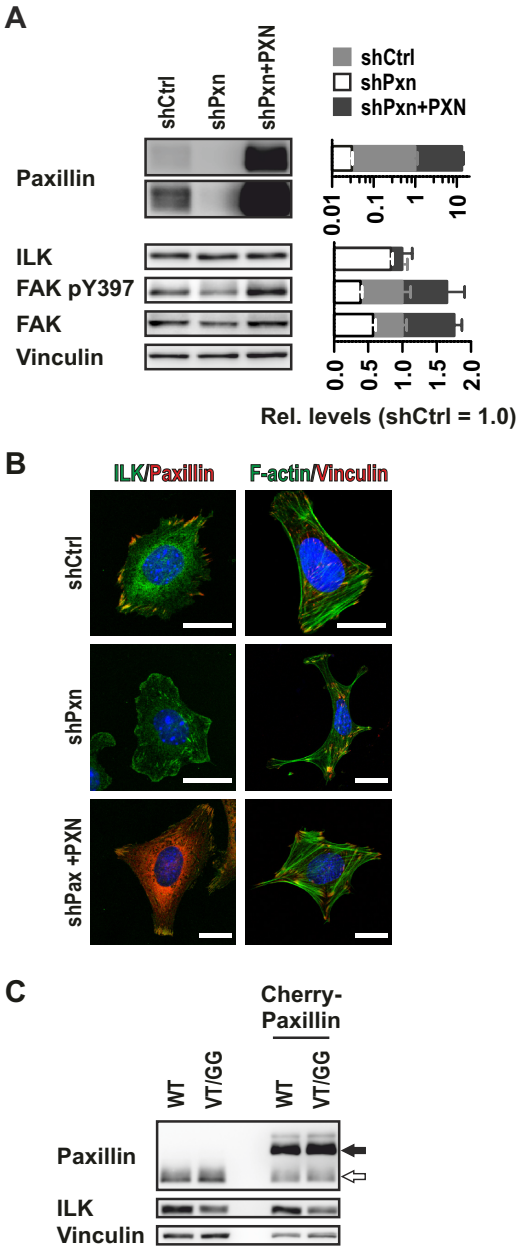

FIGURE 6. **ILK expression levels and localization are unaffected by depletion or overexpression of paxillin.** *A*, immunoblot analysis for the indicated proteins in ILK-floxed fibroblasts stably expressing control shRNA (shCtrl), paxillin-specific shRNA (shPxn), or expressing shPxn plus shPxn-resistant human paxillin (shPxn+PXN). *Left panel*, *bars* indicate mean ± S.E. ($n = 3$) ratio of signal in shCtrl (*light gray*), shPxn (*white*), or shPxn+PXN (*dark gray*) cells, normalized to vinculin and relative to shCtrl. Note the logarithmic scale for paxillin. *Rel.*, relative. *B*, immunofluorescence stainings for the indicated proteins in shCtrl, shPxn, and shPxn+PXN cells. *Colors* (*green/red*) indicate false color used in pictures, nuclei were DAPI-stained (*blue*). *Scale bar*, 20 μm. *C*, immunoblot analysis for the indicated proteins in parental or Cherry-paxillin overexpressing WT and VT/GG cells. Endogenous (*white arrow*) and transgenic (*black arrow*) paxillin are indicated.

cells, suggesting that both paxillin and Hic-5 were absent (Fig. 6*B*). Depletion of paxillin phenocopied paxillin-deficient cells (19) and showed diminished focal adhesion kinase activity, abnormal cell shape, and impaired spreading. As expected, overexpression of PXN increased focal adhesion kinase activity and cell spreading, indicating that the defects due to paxillin knockdown were specific (Fig. 6, *A* and *B*). Despite the pronounced cellular phenotypes following paxillin knockdown, ILK levels and ILK recruitment to FAs were unaffected (Fig. 6, *A* and *B*).

To test whether increasing paxillin levels stabilizes ILK-VT/GG, we stably transduced paxillin tagged with mCherry (Cherry-paxillin) into cells expressing ILK-WT or -VT/GG. Increasing paxillin levels did not change ILK-WT or ILK-VT/GG levels (Fig. 6*C*). Because changes in paxillin expression had no discernible impact on levels or subcellular localization of wild-type or mutant ILK, we conclude that the reduced paxillin binding to ILK-VT/GG plays little or no role in the defects observed in $ILK^{ki/ki}$ mice.

DISCUSSION

In the present study, we analyzed the consequences of disrupting the potential PaxBS in the pseudokinase domain of ILK *in vivo* and *in vitro*. The substitutions of Val^{386} and Thr^{387} with glycines (ILK-VT/GG) were reported to disrupt paxillin-binding and to prevent ILK-VT/GG recruitment to FAs. We show in the present paper that ILK-VT/GG mice developed vasculogenesis defects, resulting in general growth retardation and onset of lethality at midgestation. Interestingly, the VT/GG mutation severely impaired the protein stability and reduced the binding to parvin but did not affect the recruitment of ILK-VT/GG to the FAs of MEFs derived from mutant mice.

Our results differ from previous *in vitro* data, where ILK-VT/GG overexpressed in various cell lines was unable to interact with parvin and paxillin and to localize to FAs (20, 21). We could resolve this discrepancy by showing that endogenous wild-type ILK prevents FA localization of co-expressed ILK-VT/GG, whereas in absence of endogenous ILK, FA localization of ILK-VT/GG was normal. Because endogenous wild-type ILK and co-expressed mutant ILK-VT/GG apparently compete for interactors necessary for FA targeting, we conclude that ILK-VT/GG has most likely a reduced affinity to these protein(s) compared with wild-type ILK. This decrease is independent of paxillin because neither overexpression nor near-complete RNAi-mediated depletion of paxillin affected the localization of ILK. A related study has recently shown that deletion of the paxillin gene also did not prevent localization of the obligate ILK binding partner parvin to FAs (22). Although the related family member Hic-5 may have taken over the "recruitment role" of paxillin, the absence of detectable Hic-5 after RNAi-mediated paxillin depletion in our cell system argues against this possibility. Taken together, these findings suggest there is no role for paxillin in FA recruitment of ILK.

Despite the localization of ILK-VT/GG to FAs, we noted a >75% decrease of ILK-VT/GG and concomitantly of PINCH and parvin protein levels in mutant embryos and cells, which was due to an accelerated protein turnover. The decreased protein stability of ILK-VT/GG supports the notion that the amino acid substitutions destabilized folding (4). The destabilization might directly result in unfolding and degradation of ILK and/or affect ILK binding to known direct interactors such as parvin, which would indirectly promote degradation of both ILK and parvin, as both proteins expose a large hydrophobic interface in the non-bound state. Although the mutual dependence of ILK/PINCH/parvin protein stability on their interaction is well documented (6–8), there are currently no data available pointing to an involvement of paxillin in IPP complex stability. Our data revealed that ILK protein stability was unaffected upon paxillin depletion or overexpression. However, parvin protein levels were more severely decreased in mutant cells and embryos compared with ILK or PINCH. Moreover, overexpression of ILK-VT/GG failed to rescue parvin levels, whereas PINCH levels did increase. The explanation for this difference in protein stability could be the ability of ILK, but not of parvin, to directly bind the chaperone HSP90 (37, 41). Because paxillin can associate with the IPP complex through either direct binding to ILK or indirect binding to parvin, it is possible that the reduced paxillin in ILK-VT/GG immunoprecipitates is a consequence of the reduced parvin binding to ILK rather than a reduced direct binding to the PaxBS-deficient ILK.

We have previously reported that cells with a complete loss of ILK expression show impaired cell spreading and directional cell migration (13, 14). Interestingly, the >75% reduction in IPP proteins in ILK-VT/GG cells enabled adhesion and spreading but reduced the directionality of migration. This interesting observation points to a hierarchical requirement of IPP for cellular functions, with efficient directionality of cell migration requiring >25% of normal IPP levels, and cell adhesion and spreading depending on <25% of normal IPP levels. It is, however, also possible that an ILK-parvin-paxillin scaffold within FAs is required for directional cell migration but not for adhesion and spreading. The inability to rescue the cell migration defect by overexpressing ILK-VT/GG supports the latter possibility. The paxillin-parvin complex has been crystallized, and the binding interface was precisely determined and mapped (22–24). A similar endeavor carried out with *in vitro* expressed ILK/paxillin proteins could show whether such a function is principally possible to occur in FAs.

How do the alterations we observed on molecular and cell level relate to the phenotype that we observed *in vivo*? ILK-VT/GG embryos had a less severe defect than ILK-null embryos, which die at peri-implantation due to defective cell adhesion, spreading, polarity, and F-actin distribution (13). These processes were not affected in ILK-VT/GG embryos and therefore implantation also proceeded normally. Instead, we observed a general developmental delay with an onset at around E8.5 and fully penetrant embryonic lethality by E12.5, which could be explained with the prominent defects in the yolk sac vasculature. Several mouse strains showing an impaired development of the yolk sac vasculature suffer from pleiotropic defects due to insufficient nutritional supply and die at around E12.5 (38–40). The ILK-VT/GG phenotype resembled the endothelial cell-specific deletion of the ILK gene, which also resulted in a lethal vasculogenesis defect (16). Vascular development critically depends on directed migration of endothelial precursor cells (36), which is also affected in ILK-VT/GG cells. Reduced cell migration directionality upon loss of ILK in keratinocytes was also previously shown to disrupt hair follicle morphogenesis (15). We can currently only speculate if and to what extent defective cell migration contributes to the observed general developmental delay in other tissues. When considering the large phenotypic overlap with other mutants experiencing defective yolk sac development, we believe that perturbed yolk sac vasculogenesis due to defective cell migration is likely the dominant cause for the embryonic lethality.

Acknowledgments—We thank Madis Jacobson for advice regarding the analysis of embryos, Christian Biertümpfel for help with analyzing structure data, Aurelia Raducanu for support, Marc Schmidt-Supprian for providing the vector pSB-ITR_CAG-IRES-hygroR, and Lukas Huber for providing the Cherry-paxillin cDNA.

REFERENCES

1. Wickström, S. A., Radovanac, K., and Fässler, R. (2011) Genetic analyses of integrin signaling. *Cold Spring Harb. Perspect. Biol.* **3,** a005116
2. Lange, A., Wickström, S. A., Jakobson, M., Zent, R., Sainio, K., and Fässler, R. (2009) Integrin-linked kinase is an adaptor with essential functions during mouse development. *Nature* **461,** 1002–1006
3. Widmaier, M., Rognoni, E., Radovanac, K., Azimifar, S. B., and Fässler, R. (2012) Integrin-linked kinase at a glance. *J. Cell Sci.* **125,** 1839–1843
4. Chiswell, B. P., Zhang, R., Murphy, J. W., Boggon, T. J., and Calderwood, D. A. (2008) The structural basis of integrin-linked kinase-PINCH interactions. *Proc. Natl. Acad. Sci. U.S.A.* **105,** 20677–20682
5. Fukuda, K., Gupta, S., Chen, K., Wu, C., and Qin, J. (2009) The pseudoactive site of ILK is essential for its binding to α-Parvin and localization to focal adhesions. *Mol. Cell* **36,** 819–830
6. Stanchi, F., Grashoff, C., Nguemeni Yonga, C. F., Grall, D., Fässler, R., and Van Obberghen-Schilling, E. (2009) Molecular dissection of the ILK-PINCH-parvin triad reveals a fundamental role for the ILK kinase domain

in the late stages of focal-adhesion maturation. *J. Cell Sci.* **122,** 1800–1811
7. Fukuda, T., Chen, K., Shi, X., and Wu, C. (2003) PINCH-1 is an obligate partner of integrin-linked kinase (ILK) functioning in cell shape modulation, motility, and survival. *J. Biol. Chem.* **278,** 51324–51333
8. Zhang, Y., Chen, K., Tu, Y., Velyvis, A., Yang, Y., Qin, J., and Wu, C. (2002) Assembly of the PINCH-ILK-CH-ILKBP complex precedes and is essential for localization of each component to cell-matrix adhesion sites. *J. Cell Sci.* **115,** 4777–4786
9. Montanez, E., Wickström, S. A., Altstätter, J., Chu, H., and Fässler, R. (2009) α-parvin controls vascular mural cell recruitment to vessel wall by regulating RhoA/ROCK signalling. *EMBO J.* **28,** 3132–3144
10. Boulter, E., Grall, D., Cagnol, S., and Van Obberghen-Schilling, E. (2006) Regulation of cell-matrix adhesion dynamics and Rac-1 by integrin linked kinase. *FASEB J.* **20,** 1489–1491
11. Tu, Y., Li, F., and Wu, C. (1998) Nck-2, a novel Src homology2/3-containing adaptor protein that interacts with the LIM-only protein PINCH and components of growth factor receptor kinase-signaling pathways. *Mol. Biol. Cell* **9,** 3367–3382
12. Azimifar, S. B., Böttcher, R. T., Zanivan, S., Grashoff, C., Krüger, M., Legate, K. R., Mann, M., and Fässler, R. (2012) Induction of membrane circular dorsal ruffles requires co-signalling of integrin-ILK-complex and EGF receptor. *J. Cell Sci.* **125,** 435–448
13. Sakai, T., Li, S., Docheva, D., Grashoff, C., Sakai, K., Kostka, G., Braun, A., Pfeifer, A., Yurchenco, P. D., and Fässler, R. (2003) Integrin-linked kinase (ILK) is required for polarizing the epiblast, cell adhesion, and controlling actin accumulation. *Genes Dev.* **17,** 926–940
14. Lorenz, K., Grashoff, C., Torka, R., Sakai, T., Langbein, L., Bloch, W., Aumailley, M., and Fässler, R. (2007) Integrin-linked kinase is required for epidermal and hair follicle morphogenesis. *J. Cell Biol.* **177,** 501–513
15. Wickström, S. A., Lange, A., Hess, M. W., Polleux, J., Spatz, J. P., Krüger, M., Pfaller, K., Lambacher, A., Bloch, W., Mann, M., Huber, L. A., and Fässler, R. (2010) Integrin-linked kinase controls microtubule dynamics required for plasma membrane targeting of caveolae. *Dev. Cell* **19,** 574–588
16. Friedrich, E. B., Liu, E., Sinha, S., Cook, S., Milstone, D. S., MacRae, C. A., Mariotti, M., Kuhlencordt, P. J., Force, T., Rosenzweig, A., St-Arnaud, R., Dedhar, S., and Gerszten, R. E. (2004) Integrin-linked kinase regulates endothelial cell survival and vascular development. *Mol. Cell. Biol.* **24,** 8134–8144
17. Deakin, N. O., and Turner, C. E. (2008) Paxillin comes of age. *J. Cell Sci.* **121,** 2435–2444
18. Hagel, M., George, E. L., Kim, A., Tamimi, R., Opitz, S. L., Turner, C. E., Imamoto, A., and Thomas, S. M. (2002) The adaptor protein paxillin is essential for normal development in the mouse and is a critical transducer of fibronectin signaling. *Mol. Cell. Biol.* **22,** 901–915
19. Wade, R., Bohl, J., and Vande Pol, S. (2002) Paxillin null embryonic stem cells are impaired in cell spreading and tyrosine phosphorylation of focal adhesion kinase. *Oncogene* **21,** 96–107
20. Nikolopoulos, S. N., and Turner, C. E. (2001) Integrin-linked kinase (ILK) binding to paxillin LD1 motif regulates ILK localization to focal adhesions. *J. Biol. Chem.* **276,** 23499–23505
21. Nikolopoulos, S. N., and Turner, C. E. (2002) Molecular dissection of actopaxin-integrin-linked kinase-Paxillin interactions and their role in subcellular localization. *J. Biol. Chem.* **277,** 1568–1575
22. Stiegler, A. L., Draheim, K. M., Li, X., Chayen, N. E., Calderwood, D. A., and Boggon, T. J. (2012) Structural Basis for Paxillin Binding and Focal Adhesion Targeting of β-Parvin. *J. Biol. Chem.* **287,** 32566–32577
23. Lorenz, S., Vakonakis, I., Lowe, E. D., Campbell, I. D., Noble, M. E., and Hoellerer, M. K. (2008) Structural analysis of the interactions between paxillin LD motifs and α-parvin. *Structure* **16,** 1521–1531
24. Wang, X., Fukuda, K., Byeon, I. J., Velyvis, A., Wu, C., Gronenborn, A., and Qin, J. (2008) The structure of α-parvin CH2-paxillin LD1 complex reveals a novel modular recognition for focal adhesion assembly. *J. Biol. Chem.* **283,** 21113–21119
25. Gao, G., Prutzman, K. C., King, M. L., Scheswohl, D. M., DeRose, E. F., London, R. E., Schaller, M. D., and Campbell, S. L. (2004) NMR solution structure of the focal adhesion targeting domain of focal adhesion kinase in complex with a paxillin LD peptide: evidence for a two-site binding model. *J. Biol. Chem.* **279,** 8441–8451
26. Fässler, R., and Meyer, M. (1995) Consequences of lack of β1 integrin gene expression in mice. *Genes Dev.* **9,** 1896–1908
27. Betz, U. A., Vosshenrich, C. A., Rajewsky, K., and Müller, W. (1996) Bypass of lethality with mosaic mice generated by Cre-loxP-mediated recombination. *Curr. Biol.* **6,** 1307–1316
28. Jat, P. S., and Sharp, P. A. (1986) Large T antigens of simian virus 40 and polyomavirus efficiently establish primary fibroblasts. *J. Virol.* **59,** 746–750
29. Li, M. Z., and Elledge, S. J. (2007) Harnessing homologous recombination in vitro to generate recombinant DNA via SLIC. *Nat. Methods* **4,** 251–256
30. Mátés, L., Chuah, M. K., Belay, E., Jerchow, B., Manoj, N., Acosta-Sanchez, A., Grzela, D. P., Schmitt, A., Becker, K., Matrai, J., Ma, L., Samara-Kuko, E., Gysemans, C., Pryputniewicz, D., Miskey, C., Fletcher, B., VandenDriessche, T., Ivics, Z., and Izsvák, Z. (2009) Molecular evolution of a novel hyperactive Sleeping Beauty transposase enables robust stable gene transfer in vertebrates. *Nat. Genet.* **41,** 753–761
31. Moik, D. V., Janbandhu, V. C., and Fässler, R. (2011) Loss of migfilin expression has no overt consequences on murine development and homeostasis. *J. Cell Sci.* **124,** 414–421
32. Schneider, C. A., Rasband, W. S., and Eliceiri, K. W. (2012) NIH Image to ImageJ: 25 years of image analysis. *Nat. Methods* **9,** 671–675
33. Chen, D., Roberts, R., Pohl, M., Nigam, S., Kreidberg, J., Wang, Z., Heino, J., Ivaska, J., Coffa, S., Harris, R. C., Pozzi, A., and Zent, R. (2004) Differential expression of collagen- and laminin-binding integrins mediates ureteric bud and inner medullary collecting duct cell tubulogenesis. *Am. J. Physiol. Renal Physiol.* **287,** F602–611
34. Meyer, M., Müller, A. K., Yang, J., Moik, D., Ponzio, G., Ornitz, D. M., Grose, R., and Werner, S. (2012) FGF receptors 1 and 2 are key regulators of keratinocyte migration in vitro and in wounded skin. *J. Cell Sci.* **125,** 5690–5701
35. Theiler, K. (1989) *The House Mouse: Atlas of Embryonic Development*, pp. 26–112 Springer-Verlag, New York
36. Schmidt, A., Brixius, K., and Bloch, W. (2007) Endothelial precursor cell migration during vasculogenesis. *Circ. Res.* **101,** 125–136
37. Aoyagi, Y., Fujita, N., and Tsuruo, T. (2005) Stabilization of integrin-linked kinase by binding to Hsp90. *Biochem. Biophys. Res. Commun.* **331,** 1061–1068
38. Dickson, M. C., Martin, J. S., Cousins, F. M., Kulkarni, A. B., Karlsson, S., and Akhurst, R. J. (1995) Defective haematopoiesis and vasculogenesis in transforming growth factor-β 1 knock out mice. *Development* **121,** 1845–1854
39. Martin, J. S., Dickson, M. C., Cousins, F. M., Kulkarni, A. B., Karlsson, S., and Akhurst, R. J. (1995) Analysis of homozygous TGF β1 null mouse embryos demonstrates defects in yolk sac vasculogenesis and hematopoiesis. *Ann. N.Y. Acad. Sci.* **752,** 300–308
40. Oshima, M., Oshima, H., and Taketo, M. M. (1996) TGF-β receptor type II deficiency results in defects of yolk sac hematopoiesis and vasculogenesis. *Dev. Biol.* **179,** 297–302
41. Radovanac, K., Morgner, J., Schulz, J. N., Blumbach, K., Patterson, C., Geiger, T., Mann, M., Krieg, T., Eckes, B., Fässler, R., and Wickström, S. A. (2013) Stabilization of integrin-linked kinase by the Hsp90-CHIP axis impacts cellular force generation, migration and the fibrotic response. *EMBO J.* **32,** 1409–1424